APPLIED PHYSICS LETTERS **91**, 122907 (2007)

Aging-induced double ferroelectric hysteresis loops in $BiFeO_3$ multiferroic ceramic

G. L. Yuan
Department of Applied Physics, The Hong Kong Polytechnic University, Hung Hom, Kowloon, Hong Kong and Helmholtz-Institut fur Strahlen-und Kernphysik, University of Bonn, Nussallee 14-16, D-53115 Bonn, Germany

Y. Yang
Precision Driving Laboratory, Nanjing University of Aeronautics and Astronautics, Nanjing 210016, China

Siu Wing Or[a)]
Department of Applied Physics, The Hong Kong Polytechnic University, Hung Hom, Kowloon, Hong Kong

(Received 25 May 2007; accepted 28 August 2007; published online 18 September 2007)

Double ferroelectric hysteresis (P-E) loops are observed in aged $BiFeO_3$ multiferroic ceramic at room temperature and are explained according to an aging effect driven by charged defects with high activation energy. The aged $BiFeO_3$ shows $R3c$ defect symmetry and allows a nonzero charged defect-induced polarization (P_D) below the ferroelectric Curie temperature. This P_D is strong enough to recover the switched 180° ferroelectric domains upon the removal of E, but it is rather weak to effectively switch back the 71°/109° ferroelectric domains. As a result, the traits of the double P-E loops weaken with increasing the maximum E from 121 to 167 kV/cm. © *2007 American Institute of Physics*. [DOI: 10.1063/1.2786013]

Single-phase $BiFeO_3$ is a multiferroic ceramic famous for the presence of both ferroelectric order below a high Curie temperature ($T_{C\text{-FE}}$) of ~830 °C and G-type canted antiferromagnetic order below a high Néel temperature ($T_{N\text{-AFM}}$) of ~370 °C.[1–4] Like other multiferroic ceramics (e.g., $TbMnO_3$, $DyMnO_3$, $Tb_{1-x}Dy_xMnO_3$, $WMnO_4$, $TbMn_2O_5$, and YMn_2O_5),[5–7] the spiral spin order of $BiFeO_3$ may induce an additional (small) polarization, being sensitive to applied magnetic fields.

While there are many reports on the structural, dielectric, and ferroelectromagnetic properties of $BiFeO_3$ multiferroic ceramic in recent years,[1–4] few reports are made on the aging effect, particularly on the aging-induced double ferroelectric hysteresis effect. In ABO_3-type ferroelectric ceramics, the observed double ferroelectric hysteresis (P-E) loops mainly result from antiferroelectric components, electric field-induced paraelectric-ferroelectric (PE-FE) phase transition near $T_{C\text{-FE}}$, and/or an aging effect far below $T_{C\text{-FE}}$. However, there is no direct indication (e.g., superhigh stress, supersmall crystal grain, excess doping, etc.) of the appearance of antiferroelectric components in $BiFeO_3$.[8] Besides, the double P-E loops reported so far in $BaTiO_3$- and $(BiNa)TiO_3$-based ceramics are at temperatures near $T_{C\text{-FE}}$,[9,10] yet those found in aged doped $BaTiO_3$/$(BaSr)TiO_3$ crystals or ceramics are far below $T_{C\text{-FE}}$.[11–14] These give essential evidences that aging may induce double P-E loops in $BiFeO_3$ at room temperature. In this letter, we explain the double P-E loops observed in the aged $BiFeO_3$ at room temperature according to a special aging effect adopted by Ren and co-workers.[11–14]

A rapid liquid-phase sintering technique was used to prepare single-phase $BiFeO_3$ ceramic.[2,15] High-purity Bi_2O_3 and Fe_2O_3 powders of <1 μm size were mixed thoroughly and pressed uniaxially into disk samples with a diameter of 5 mm and a thickness of 1.2 mm. The samples were sintered at 855 °C for 20 min at high heating and cooling rates of 100 and 10 °C/s, respectively.

The crystal structure of the freshly sintered sample (denoted as "fresh sample") was examined by an x-ray diffractometer (Brucker D8 Advance System) with a 2θ step size of 0.02° and at a scan rate of one step/4 s. Simulation of crystal structure based on the measured x-ray diffraction (XRD) data was performed using a Rietveld crystal structure refinement software (FULLPROF 2000). The fresh sample was thinned down to 0.4 mm thick, and silver paste was applied on its two major surfaces as electrodes. The ferroelectric hysteresis (P-E) loops of the fresh sample were measured with a standard Sawyer-Tower circuit at 100 Hz. The electric field dependence of leakage current density (J-E) of the sample was evaluated using a multimeter (Keithley 2000) and a high-voltage amplifier (Trek P0621P). The relative dielectric constant (ε) and loss tangent ($\tan\delta$) were determined from 100 Hz to 1 MHz by an impedance analyzer (Agilent 4294A) and from 0.01 Hz to 1 MHz by a broadband dielectric spectrometer (Novocontrol Concept80). The fresh sample was exposed to an environmental chamber for aging at 150 °C for 5 days, and the resulting sample is denoted as "aged sample." The above measurements were repeated for the aged sample.

Figure 1 shows the comparison between the measured and simulated XRD patterns of the fresh $BiFeO_3$ sample. The refined crystal parameters (i.e., $a=b=c=0.3942$ nm and $\alpha=\beta=\gamma=89.43°$) coincide well with the previous reports about the existence of a rhombohedral structure with the $R3c$ space group in single-phase bulk $BiFeO_3$ at room temperature.[2,15]

Figure 2 plots the measured ferroelectric hysteresis (P-E) loops of the fresh and aged $BiFeO_3$ samples at room temperature. The fresh sample shows single P-E loops at two different maximum electric fields (E_m) of 121 and 151 kV/cm [Fig. 2(a)]. These single P-E loops become

[a)]Electronic mail: apswor@polyu.edu.hk

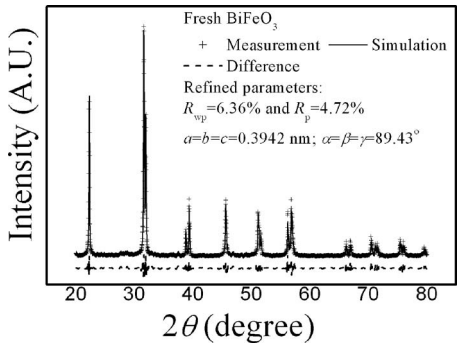

FIG. 1. Comparison between the measured and simulated XRD patterns of the fresh $BiFeO_3$ sample.

double *P-E* loops after the fresh sample is aged at 150 °C for 5 days [Fig. 2(b)]. The arrow lines in Fig. 2(b) project the possible tracks of the single *P-E* loops based on the measured double *P-E* loops. The change from the single *P-E* loops in the fresh sample to the double *P-E* loops in the aged sample should exclude the antiferroelectric components and the electric field-induced PE-FE phase transition near $T_{C\text{-FE}}$ from the main cause since both samples should experience the same effect from them. Referring to Fig. 2(b), the difference in polarization between a measured double *P-E* loop and a projected single *P-E* loop is denoted as ΔP. This ΔP remains quite constant in the first-order approximation compared to the rapid increase in P_S with increasing E_m from 121 to 167 kV/cm. Accordingly, weakening of the traits of the double *P-E* loops (i.e., $\Delta P/P_S$) increases with increasing E_m.

Figure 3 shows the measured electric field dependence of leakage current density (*J-E*) and frequency dependence of relative dielectric constant (ε-*f*) and loss tangent (tan δ-*f*) of the fresh and aged samples at room temperature. From Fig. 3(a), both samples have similarly low *J* of <35 mA/m^2

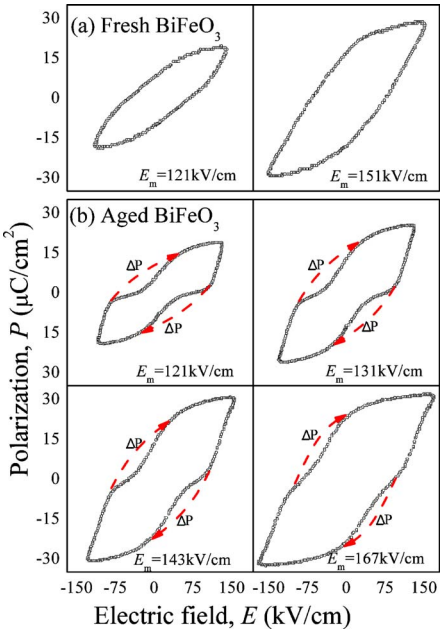

FIG. 2. (Color online) Measured ferroelectric hysteresis (*P-E*) loops of the fresh and aged $BiFeO_3$ samples at room temperature. (a) Fresh sample with single *P-E* loops at the maximum electric fields (E_m) of 121 and 151 kV/cm, and (b) aged sample with double *P-E* loops at E_m of 121, 131, 143, and 167 kV/cm.

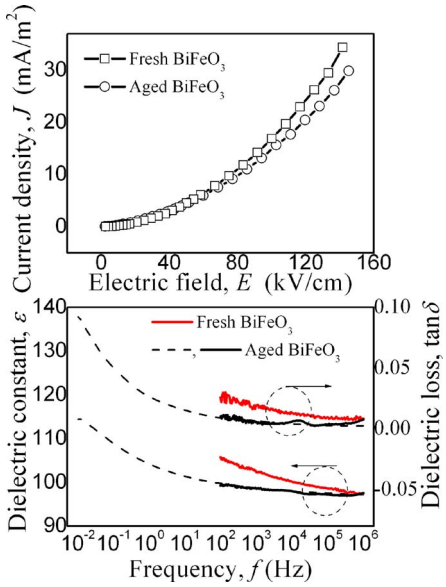

FIG. 3. (Color online) (a) Measured electric field dependence of leakage current density (*J-E*) and (b) measured frequency dependence of relative dielectric constant (ε-*f*) and loss tangent (tan δ-*f*) of the fresh and aged $BiFeO_3$ samples at room temperature.

even though they are subject to an elevated *E* in excess of 140 kV/cm. This reasonably low *J* not only provides an important proof of the presence of charged defects with high activation energy (corresponding to those trapped in deep potential wells) in both samples but also is a precondition for observing true single and double *P-E* loops in our samples in Fig. 2 (to be discussed later).[15] In Fig. 3(b), the slight decrease in ε from 106 to 98 and the generally low tan δ of <0.03 in the fresh sample imply a more significant contribution of electrons/domains than charged defects to the characteristics of ε and tan δ in the higher *f* range of 100 Hz–1 MHz. The aged sample, which has relatively stable and smaller values of ε and tan δ, demonstrates convergence trends toward 1 MHz with the fresh sample. This suggests a weaker contribution from charged defects in the aged sample for $f>100$ Hz. An extrinsic factor for the general reduction in ε and tan δ with decreasing *f* and in *J* with increasing *E* in the aged sample compared to the fresh sample is the reduced water vapor content after the 150 °C aging. An intrinsic factor comes from the different distributions of charged defects, i.e., a random distribution in the fresh sample and a special distribution with the *R*3*c* defect symmetry in the aged sample (to be discussed later).

The double *P-E* loops observed in Fig. 2 can be explained according to a special aging effect related to the defect symmetry defined as the conditional probability of finding O^{2-} vacancies at site *i* ($i=1-6$) of an ABO_3 single cell.[11–14] In this case, the amount of the induced charged defects with high activation energy should not be too low in order to produce a sufficiently large charged defect-induced polarization (P_D).[11–14] This is why the double *P-E* loops are observable in our aged sample. Figure 4 depicts how the double *P-E* loops are produced in a single-crystal grain of the aged $BiFeO_3$ sample.[11,14] Some associated remarks are included as follows.

(1) When the $BiFeO_3$ fresh sample is just sintered and its temperature (*T*) is still above $T_{C\text{-FE}}$, its single-crystal grain exhibits an *m*3*m* crystal symmetry and an *m*3*m*

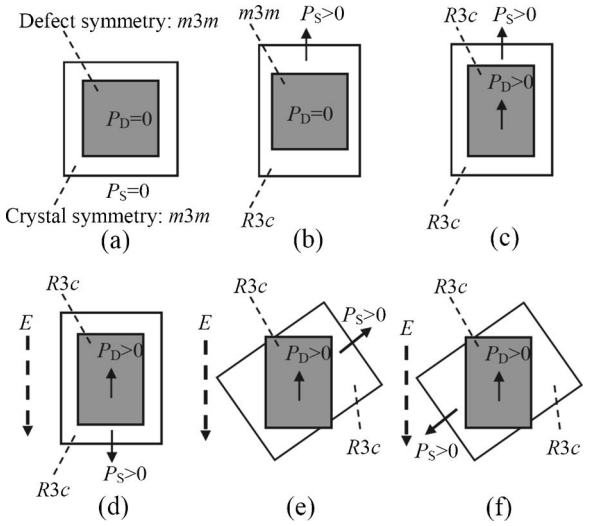

FIG. 4. Crystal symmetry and defect symmetry of a single-crystal grain in (a) a fresh $BiFeO_3$ sample at $T>T_{C\text{-FE}}$, (b) the fresh sample at $T<T_{C\text{-FE}}$, and (c) the aged sample at room temperature. (d), (e), and (f) show the electric field (E)-induced switching of the 180°, 71°, and 109° ferroelectric domains, respectively, in the aged sample at room temperature.

defect symmetry, giving rise to zero P_S and P_D [Fig. 4(a)].

(2) At $T<T_{C\text{-FE}}$, the PE-FE phase transition leads to a rhombohedral $R3c$ crystal symmetry, producing a nonzero P_S (i.e., $P_S>0$) [Fig. 4(b)]. However, there does not appear to be any change in the $m3m$ defect symmetry due to the slower defect diffusion in comparison with the PE-FE phase transition. In general, a pyrostrain is induced from the difference between the $R3c$ crystal symmetry and the $m3m$ defect symmetry.

(3) When the fresh sample is being aged at 150 °C for 5 days, diffusion of the available charged defects, especially for the O^{2-} vacancies with the smallest effective mass and ion radius, occurs with the help of both the difference in symmetry and the induced pyrostrain as mentioned in (2). At an equilibrium state, the positively charged centers of Bi^{3+} vacancies and Fe^{2+} ions separate from the negatively charged center of O^{2-} vacancies, leading to a $R3c$ defect symmetry and a nonzero P_D [Fig. 4(c)]. Since this $R3c$ defect symmetry is the same as the rhombohedral $R3c$ crystal symmetry, the resulting P_D is along the direction of P_S in the single-crystal grain.[11–14]

(4) By applying an electric field (E) with the maximum amplitude (E_m) of 121–167 kV/cm and of a frequency ⩾100 Hz parallel and opposite to the direction of P_S and P_D as in Fig. 4(c), it can induce an effective switching of the available 180° ferroelectric domains with small coercivity ($E_{C\text{-}80}$) so that a 180° reversal of P_S with respect to P_D occurs [Fig. 4(d)]. As the diffusion of the charged defects is minimal, both the $R3c$ defect symmetry and P_D are preserved. Upon the removal of E, the status of Fig. 4(c) is recovered by a restoring E of P_D, being larger than $2E_{C\text{-}180}$ (i.e., twice the coercivity of the 180° ferroelectric domains). This 180° ferroelectric domain switching contributes to a constant ΔP and hence to the double P-E loops, as seen in Fig. 2(b).

(5) Under such an applied E, and if the diffusion of the charged defects is still minimal, the 71°/109° ferroelectric domain switching can induce an electrostrain because of the difference in azimuth angle between the $R3c$ crystal symmetry and the $R3c$ defect symmetry [Figs. 4(e) and 4(f)].[11,14] Similarly, the status of Fig. 4(c) can be recovered after removing E, provided that the restoring E of P_D is larger than $2E_{C\text{-}71/109}$ (i.e., twice the coercivity of the 71°/109° ferroelectric domains). The switching of the 71°/109° ferroelectric domains results in the double P-E loops and a large recoverable electrostrain.[12] In our aged sample, however, the restoring E of P_D may be smaller than $2E_{C\text{-}71/109}$ in the first-order approximation. This implies that a reverse switching of the 71°/109° ferroelectric domains from Figs. 4(e) or 4(f) and 4(c) may be difficult, and the switching of the 71°/109° ferroelectric domains mainly benefits P_S rather than ΔP for E_m varying from 121 to 167 kV/cm, as evidenced in Fig. 2(b).

It is noted that the corresponding pinned defects of ABO_3-type ferroelectric ceramics can be unpinned by a high-temperature annealing, a large dc field, or a low-frequency ac field. Thus, the use of a higher-frequency ac field and a relatively low E_m is favorable to nondestructively measure the double P-E loops.

In conclusion, double P-E loops have been observed in the aged single-phase $BiFeO_3$ multiferroic ceramic at room temperature. Charged defects with high activation energy form $R3c$ defect symmetry, besides producing a nonzero P_D, in the aged sample below $T_{C\text{-FE}}$. The restoring E of P_D, which is larger than $2E_{C\text{-}180}$, is strong enough to restore the initially switched 180° ferroelectric domains upon the removal of the applied E. However, it is rather weak to effectively recover the switched 71°/109° ferroelectric domains. Therefore, weakening of the traits of the double P-E loops increases with increasing E_m from 121 to 167 kV/cm.

This work was supported by the Innovation and Technology Fund of the HKSAR Government (GHP/003/06), Alexander von Humboldt Foundation, and National Natural Science Foundation of China (50572038). Technical advice from Dr. Shantao Zhang is also acknowledged.

[1] M. Fiebig, J. Phys. D **38**, R123 (2005).
[2] G. L. Yuan, S. W. Or, J. M. Liu, and Z. G. Liu, Appl. Phys. Lett. **89**, 052905 (2006).
[3] B. Ruette, S. Zvyagin, A. P. Pyatakov, A. Bush, J. F. Li, V. I. Belotelov, A. K. Zvezdin, and D. Viehland, Phys. Rev. B **69**, 064114 (2004).
[4] T. Zhao, A. Scholl, F. Zavaliche, K. Lee, M. Barry, A. Doran, M. P. Cruz, Y. H. Chu, C. Ederer, N. A. Spaldin, R. R. Das, D. M. Kim, S. H. Baek, C. B. Eom, and R. Ramesh, Nat. Mater. **5**, 823 (2006).
[5] K. Taniguchi, N. Abe, T. Takenobu, Y. Iwasa, and T. Arima, Phys. Rev. Lett. **97**, 097203 (2006).
[6] M. Mostovoy, Phys. Rev. Lett. **96**, 067601 (2006).
[7] S. W. Cheong and M. Mostovoy, Nat. Mater. **6**, 13 (2007).
[8] D. H. Kim, H. N. Lee, M. Varela, and H. M. Christen, Appl. Phys. Lett. **89**, 162904 (2006).
[9] N. Srivastava and G. J. Weng, J. Appl. Phys. **99**, 054103 (2006).
[10] T. Oh, Jpn. J. Appl. Phys., Part 1 **45**, 5138 (2006).
[11] L. X. Zhang, W. Chen, and X. B. Ren, Appl. Phys. Lett. **85**, 5658 (2004).
[12] D. Sun, X. B. Ren, and K. Otsuka, Appl. Phys. Lett. **87**, 142903 (2005).
[13] W. F. Liu, W. Chen, L. Yang, L. X. Zhang, Y. Wang, C. Zhou, S. T. Li, and X. B. Ren, Appl. Phys. Lett. **89**, 172908 (2006).
[14] L. X. Zhang and X. B. Ren, Phys. Rev. B **73**, 094121 (2006).
[15] G. L. Yuan and S. W. Or, Appl. Phys. Lett. **88**, 062905 (2006).